J|A|C|S
ARTICLES

Published on Web 06/29/2010

Anisotropic and Inhomogeneous Magnetic Interactions Observed in All-Organic Nitroxide Radical Liquid Crystals

Yoshiaki Uchida,* Katsuaki Suzuki, Rui Tamura,* Naohiko Ikuma, Satoshi Shimono, Yohei Noda, and Jun Yamauchi

Graduate School of Human and Environmental Studies, Kyoto University, Kyoto 606-8501, Japan

Received March 8, 2010; E-mail: Yoshiaki.Uchida@h02.mbox.media.kyoto-u.ac.jp; tamurarui@hes.mbox.media.kyoto-u.ac.jp

Abstract: An anisotropic and inhomogeneous magnetic interaction (the average spin−spin interaction constant $\bar{J} > 0$) was observed in the various liquid crystalline (LC) phases of racemic and nonracemic all-organic radical LC compounds **1a** and **1b**. We discussed how the LC superstructures induced the magnetic interaction to operate in the LC phases in terms of spin−spin dipole and exchange interactions by means of VT-EPR spectroscopy. The magnitude of the magnetic interaction depended on the type of LC phase, or the superstructure. Furthermore, these radical LC droplets floating on water were commonly attracted to a permanent magnet and moved freely under the influence of this magnet, whereas the crystallized particles of the same compounds never responded to the magnet. The response of the LC droplets to the magnet also varied depending on the type of LC phase, that is, the extent of the magnetic interaction.

Introduction

Liquid crystals are a unique soft matter that combines fluidity and anisotropy. By taking advantage of this property, beyond prominent display uses, there are many potential applications of liquid crystalline (LC) materials such as optical data storage devices, biomedical tools, and semiconductors.[1] In this regard, paramagnetic liquid crystalline (PLC) materials have attracted great interest as soft materials to enhance the effect of magnetic fields on the electric and optical properties of liquid crystals.[2] For example, PLC materials are expected to show unique magnetic interactions and thereby unconventional magneto-electric or magneto-optical properties in the LC state,[3−6] affording the following possibilities; (i) formation of magnetic domains in applied magnetic fields and (ii) occurrence of interactions between magnetic-dipole and electric-dipole moments (magneto-electric effects)[7] in the ferroelectric LC (FLC) state, together with (iii) realization of paramagnetic susceptibility anisotropy ($\Delta\chi_{para}$)-controlled molecular orientation by weak magnetic fields. Although the possibility of a ferromagnetic LC material has been considered to be unrealistic due to the inaccessibility of long-range spin−spin interactions between rotating molecules in the LC state,[4] it is interesting to clarify whether LC domains can help to induce the formation of magnetic domains in magnetic fields. If the PLC phases tend to show any magnetic ordering in a magnetic field, the magneto-electric effects may be observed in the FLC state.

PLC materials are classified into two categories; the majority were the metallomesogens with permanent spins originating from the transition (d-orbital) or lanthanide (f-orbital) metal ion in the mesogen core,[8,9] while only a few all-organic LC materials containing an organic spin center were prepared,[4−6,10,11] because the geometry and bulkiness of the radical-stabilizing substituents are unfavorable for the stability of LC phases, which requires molecular linearity and/or planarity. The large $\Delta\chi_{para}$ of metallomesogens arising from the spin−orbital coupling seems advantageous to the orientation control of LC molecules by magnetic fields.[8,9] However, the ligand-coordinated metal complex structure frequently renders the response to weak magnetic fields difficult because of the high viscosity and tends

(1) (a) Tschierske, C. *J. Mater. Chem.* **2008**, *18*, 2869–2871. (b) Feringa, B. L.; Jager, W. F.; de Lange, B. *Tetrahedron* **1993**, *49*, 8267–8310. (c) *Liquid Crystals: Frontiers in Biomedical Applications*; Woltman, S. J., Jay, G. D., Crawford, G. P., Eds.; World Scientific: Singapore, 2007. (d) Kippelen, B.; Yoo, S.; Haddock, J. A.; Domercq, B.; Barlow, S.; Minch, B.; Xia, W.; Marder. S. R.; Armstrong, N. R. In *Organic Photovoltaics: Mechanism, Materials and Devices*; Sun, S.-S.; Sacriciftci, N. S., Eds.; CRC Press: Boca Raton, FL, 2005; Chapter 11, p 271.

(2) Blinov, L. M. *Electro-Optical and Magneto-Optical Properties of Liquid Crystals*; John Wiley & Sons: New York, 1983.

(3) (a) Griesar, K.; Haase, W. In *Magnetic Properties of Organic Molecules*; Lahti, P. M., Ed.; Marcel Dekker: New York, 1999; Chapter 16, p 325. (b) Serrano, J.-L. *Metallomesogens: Synthesis, Properties, and Applications*; VCH: Weinheim, 1996.

(4) (a) Kaszynski, P. In *Magnetic Properties of Organic Molecules*; Lahti, P. M., Ed.; Marcel Dekker: New York, 1999; Chapter 15, p 305. (b) Dunmur, D.; Tokoroyama, K. In *Physical Properties of Liquid Crystals*; Demus, D., Goodby, J., Gray, G. W., Spiess, H.-W., Vill, V., Eds.; Wiley-VCH: Weinheim, 1999; Chapter IV-2, p 102.

(5) Likhtenshtein, G. I.; Yamauchi, J.; Nakatsuji, S.; Smirnov, A. I.; Tamura, R. *Nitroxides: Applications in Chemistry, Biochemistry, and Materials Science*; Wiley-VCH: Weinheim, 2008; Chapter 9, p 303.

(6) Tamura, R.; Ikuma, N.; Shimono, S. In *Soft Nanomaterials*; Nalwa, H. S., Ed.; American Scientific Publishers, CA, 2009; Vol. 1,Chapter 8, p 257.

(7) (a) Saito, M.; Ishikawa, K.; Konno, S.; Taniguchi, K.; Arima, T. *Nat. Mater.* **2009**, *8*, 634–638. (b) Felser, C.; Fecher, G. H.; Balke, B. *Angew. Chem., Int. Ed.* **2007**, *46*, 668–699. (c) Rao, C. N. R.; Serrao, C. R. *J. Mater. Chem.* **2007**, *17*, 4931–4938. (d) Eerenstein, W.; Mathur, N. D.; Scott, J. F. *Nature* **2006**, *442*, 759–765. (e) Fiebig, M. *J. Phys. D: Appl. Phys.* **2005**, *38*, R123–R152.

 10.1021/ja101930d

to exhibit superexchange interactions between neighboring spins, often inducing antiferromagnetic interactions.[8,9] In fact, no appreciable intermolecular ferromagnetic interaction has been observed in these metallomesogens. On the other hand, all-organic rod-like LC materials with a stable nitroxyl group, which can benefit from the low viscosity and small molecular size, may form magnetic domains owing to the swift coherent collective properties of organic molecules in the LC state and thereby may show unique intermolecular magnetic interactions, although their $\Delta\chi_{para}$ is too small to control the molecular orientation by magnetic fields due to the p-orbital origin.[11]

In this context, we had synthesized prototypic all-organic radical LC compounds **1**, which (i) contain a polar and chiral cyclic-nitroxide unit in the mesogen core, (ii) are thermally stable up to 150 °C in the air and (iii) can show LC phases over a wide temperature range below 90 °C (Figure 1).[12−14] As a preliminary result, by measuring the temperature dependence of molar magnetic susceptibility (χ_M) on a SQUID magnetometer, a considerable net increase in paramagnetic susceptibility (χ_{para}) was observed in the SmC phase of (±)-**1a** in a weak magnetic field, suggesting the induction of an unusual magnetic interaction in the LC superstructures.[6,10,13] Furthermore, the LC droplet of the same SmC phase floating on water was attracted by a permanent magnet and moved freely on water under the influence of this magnet, whereas the crystallized particle never moved under the same magnet.[6,10,13]

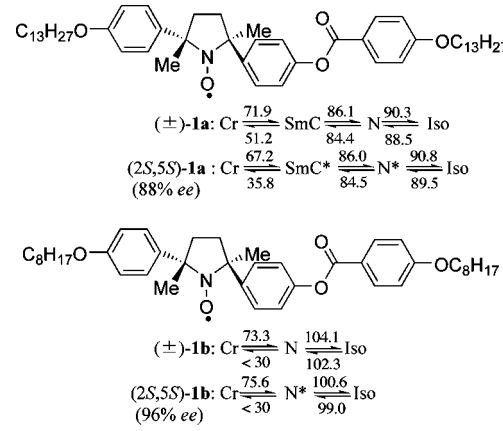

Figure 1. Molecular structures and phase transition temperatures determined by DSC analysis of racemic and (2*S*,5*S*)-enriched **1**. Cr, SmC, SmC*, N, N*, and Iso denote the crystalline, smectic C, chiral smectic C, nematic, chiral nematic, and isotropic phases, respectively.

Here, we report that such an unusual magnetic interaction induced in the LC superstructure is commonly observed in all of the chiral and achiral LC phases of compounds **1a** and **1b** and then discuss the origin of this induced magnetic interaction in their LC state on the basis of (i) the magnetic-field dependence of magnetization measured on a SQUID magnetometer, (ii) the temperature (*T*) dependence of χ_{para}, *g*-value, and peak-to-peak line width (ΔH_{pp}) obtained by EPR spectroscopy, and (iii) the difference in the response of these PLC droplets floating on water to a permanent magnet (Figure 1).

Results and Discussion

SQUID Magnetometry. We had reported that racemic or (2*S*,5*S*)-enriched **1a** and **1b** showed achiral SmC and/or N phases, or chiral SmC* and/or N* phases, respectively, at ∼77 °C in the heating runs (Figure 1).[12] The magnetic-field (*H*) dependence of molar magnetization (*M*) was measured on a SQUID magnetometer using a paramagnetic aluminum pan to minimize the experimental error at high temperatures. However, we cannot exactly determine the paramagnetic magnetization (M_{para}) and susceptibility (χ_{para}) in the PLC phases, as the diamagnetic susceptibility (χ_{dia}) in the PLC phases is temperature-dependent;[15] this is because the PLC molecules with viscous fluidity and larger diamagnetic susceptibility anisotropy ($|\Delta\chi_{dia}| > |\Delta\chi_{para}|$) derived from aromatic rings exhibit a temperature-dependent molecular motion and a magnetic-field-dependent reorientation, respectively.[14,15] For this reason, in this paper we defined (i) the sum of χ_{para} and χ_{dia} as molar magnetic susceptibility ($\chi_M = \chi_{para} + \chi_{dia}$) and (ii) the sum of paramagnetic and diamagnetic magnetizations as M ($= M_{para} + M_{dia}$).

All of the four LC phases of **1a** and **1b** did not show a linear relation between *H* and *M* but drew an S-curve that passed through the origin (Figure 2), indicating no spontaneous magnetization. The magnetization highly deviated from the linearity under weak magnetic fields, implying the generation of an unusual magnetic interaction in applied magnetic fields. No magnetization saturation was observed below 5 T at 77 °C. In contrast, such a nonlinear paramagnetic magnetization (NPM) was not observed in the crystalline phases of the same compounds, which showed a usual linear relationship indicating a paramagnetic nature and no contamination of magnetic impurities in the samples (Figure S1).

(8) (a) Seredyuk, M.; Gaspar, A. B.; Ksenofontov, V.; Galyametdinov, Y.; Kusz, J.; Gütlich, P. *Adv. Funct. Mater.* **2008**, *18*, 2089–2101. (b) Galyametdinov, Y. G.; Haase, W.; Malykhina, L.; Prosvirin, A.; Bikchantaev, I.; Rakhmatullin, A.; Binnemans, K. *Chem.−Eur. J.* **2001**, *7*, 99–105. (c) Binnemans, K.; Galyametdinov, Y. G.; Deun, R. V.; Bruce, D. W.; Collinson, S. R.; Polishchuk, A. P.; Bikchantaev, I.; Haase, W.; Prosvirin, A. V.; Tinchurina, L.; Litvinov, I.; Gubajdullin, A.; Rakhmatullin, A.; Uytterhoeven, K.; Meervelt, L. V. *J. Am. Chem. Soc.* **2000**, *122*, 4335–4344. (d) Mironov, V. S.; Galyametdinov, Y. G.; Ceulemans, A.; Binnemans, K. *J. Chem. Phys.* **2000**, *113*, 10293–10303. (e) Galyametdinov, Y.; Athanassopoulou, M. A.; Griesar, K.; Kharitonova, O.; Soto Bustamante, E. A.; Tinchurina, L.; Ovchinnikov, I.; Haase, W. *Chem. Mater.* **1996**, *8*, 922–926. (f) Haase, W.; Griesar, K.; Soto Bustamante, E. A.; Galyametdinov, Y. *Mol. Cryst. Liq. Cryst.* **1995**, *274*, 99–111. (g) Griesar, K.; Galyametdinov, Y.; Athanassopoulou, M.; Ovchinnikov, I.; Haase, W. *Adv. Mater.* **1994**, *6*, 381–384.
(9) Galyametdinov, Y. G.; Haase, W.; Goderis, B.; Moors, D.; Driesen, K.; Deun, R. V.; Binnemans, K. *J. Phys. Chem. B* **2007**, *111*, 13881–13885.
(10) Tamura, R.; Uchida, Y.; Ikuma, N. *J. Mater. Chem.* **2008**, *18*, 2872–2876.
(11) (a) Castellanos, S.; Lopez-Calahorra, F.; Brillas, E.; Julia, L.; Velasco, D. *Angew. Chem., Int. Ed.* **2009**, *48*, 6516–6519. (b) Yelamaggad, C. V.; Achalkumar, A. S.; Rao, D. S. S.; Nobusawa, M.; Akutsu, H.; Yamada, J.; Nakatsuji, S. *J. Mater. Chem.* **2008**, *18*, 3433–3437. (c) Nakatsuji, S.; Mizumoto, M.; Ikemoto, H.; Akutsu, H.; Yamada, J. *Eur. J. Org. Chem.* **2002**, 1912–1918. (d) Allgaier, J.; Finkelmann, H. *Macromol. Chem. Phys.* **1994**, *195*, 1017–1030. (e) Dvolaitzky, M.; Taupin, C.; Poldy, F. *Tetrahedron Lett.* **1975**, 1469–1472. (f) Dvolaitzky, M.; Billard, J.; Poldy, F. *Tetrahedron* **1976**, *32*, 1835–1838. (g) Dvolaitzky, M.; Billard, J.; Poldy, F. *C. R. Acad. Sci. Paris, Ser. C* **1974**, *279*, 533–535.
(12) (a) Ikuma, N.; Tamura, R.; Shimono, S.; Kawame, N.; Tamada, O.; Sakai, N.; Yamauchi, J.; Yamamoto, Y. *Angew. Chem., Int. Ed.* **2004**, *43*, 3677–3682. (b) Ikuma, N.; Tamura, R.; Shimono, S.; Uchida, Y.; Masaki, K.; Yamauchi, J.; Aoki, Y.; Nohira, H. *Adv. Mater.* **2006**, *18*, 477–480. (c) Ikuma, N.; Tamura, R.; Masaki, K.; Uchida, Y.; Shimono, S.; Yamauchi, J.; Aoki, Y.; Nohira, H. *Ferroelectrics* **2006**, *343*, 119–125.
(13) Uchida, Y.; Ikuma, N.; Tamura, R.; Shimono, S.; Noda, Y.; Yamauchi, J.; Aoki, Y.; Nohira, H. *J. Mater. Chem.* **2008**, *18*, 2950–2952.
(14) Uchida, Y.; Tamura, R.; Ikuma, N.; Shimono, S.; Yamauchi, J.; Shimbo, Y.; Takezoe, H.; Aoki, Y.; Nohira, H. *J. Mater. Chem.* **2009**, *19*, 415–418.
(15) Müller, H. J.; Haase, W. *J. Phys. (Paris)* **1983**, *44*, 1209–1213.

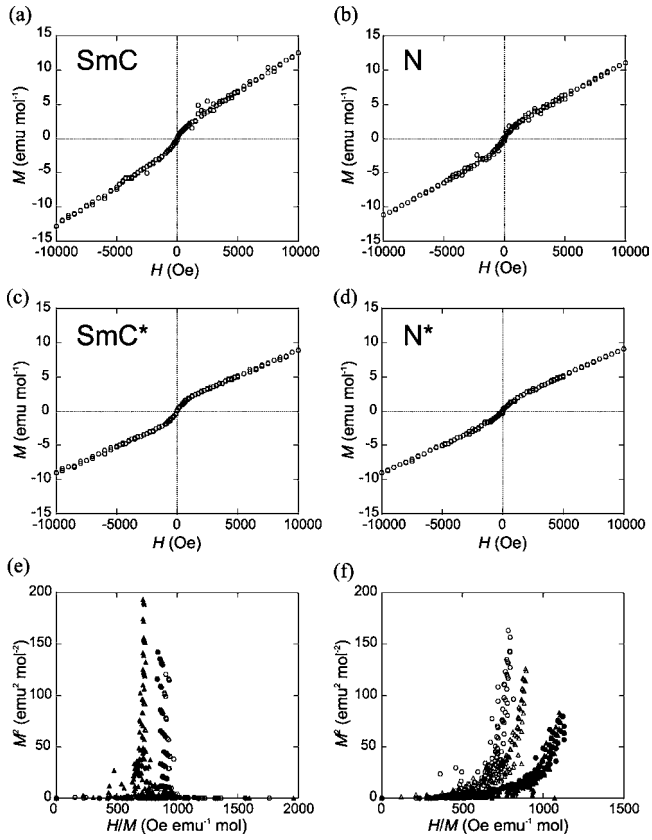

Figure 2. Magnetic field (H) dependence of molar magnetization (M) at 77 °C for (a) the SmC phase of (±)-**1a**, (b) the N phase of (±)-**1b**, (c) the SmC* phase of (2*S*,5*S*)-**1a** (88% *ee*), and (d) the N* phase of (2*S*,5*S*)-**1b** (96% *ee*), and M^2-H/M plots at 77 °C for (e) the crystalline phases and (f) the LC phases of **1a** and **1b**. In panels e and f, open and filled circles represent (±)-**1a** and (2*S*,5*S*)-**1a**, respectively, and open and filled triangles represent (±)-**1b** and (2*S*,5*S*)-**1b**, respectively.

The Brillouin function curve analysis to determine the net spin state in the PLC phases was infeasible due to the variable χ_{dia} and no magnetization saturation below 5 T in the LC state at high temperatures. Therefore, to evaluate the NPM behavior in a weak magnetic field, we plotted M^2 as a function of H/M (Arrott−Belov−Kouvel plots)[16] for respective crystalline and PLC phases of all compounds. In these crystalline phases, the M^2-H/M plots showed straight lines almost parallel to the M^2 axis (Figure 2e), indicating that the H/M which is equal to reciprocal molar magnetic susceptibility ($1/\chi_M$) is constant and thereby that the χ_M in the crystalline phases is independent of H. Meanwhile, in the PLC phases the plots showed distinct concave curves for all compounds (Figure 2f). If a molecular orientation affected the magnetization behavior, the H/M would decrease with increasing M^2. As a result, this possibility was denied because the H/M increased with increasing M^2. Therefore, it is concluded that the observed concave curve is most likely to result from the generation of a sort of spin glass (SG)-like inhomogeneous magnetic interactions (the average spin−spin interaction constant $\bar{J} > 0$).[15]

To directly prove that the magnetic behavior in the PLC phases is different from that in their crystalline phases, we measured the temperature dependence of χ_M for **1a** and **1b** at a magnetic field of 0.05 or 0.5 T (Figures S2−S5).[13] The χ_M-T plots obeyed the Curie−Weiss law in the temperature range between −173 and +40 °C [$\chi_M = \chi_{para} + \chi_{dia} = C/(T - \theta) + \chi_{dia}$: Weiss constants $\theta = -1.0$, −3.3, −0.19, and −3.2 K and Curie constants $C = 0.40$, 0. 37, 0.39, and 0.38 emu K mol^{-1} for (±)-**1a**, (±)-**1b**, (2*S*,5*S*)-**1a** (88% *ee*), and (2*S*,5*S*)-**1b** (96% *ee*), respectively, at 0.5 T] (Figures S2a,c−S5a,c), exhibiting the magnetic properties of ordinary paramagnetic radical crystals with weak antiferromagnetic interactions at lower temperatures. However, for all of these compounds between 25 and 115 °C, we observed (1) a considerable χ_M increase at the Cr-to-LC phase transition and (2) an increasing χ_M value with decreasing magnetic field in the LC phases (Figures S2d,e−S5d,e). This latter result is very consistent with that of magnetic-field dependence of magnetization in the LC phases (Figure 2). As a typical example of χ_M-T plots, as previously reported, (±)-**1a** exhibited a net χ_M increase (1.6×10^{-4} emu mol^{-1}, 16%) at 72 °C at 0.5 T between the Curie−Weiss fitting curves in the crystalline phase between −73 and 57 °C in the heating run ($\theta = -1.0$ K, $C = 0.40$ emu K mol^{-1}, and $\chi_{dia} = -2.76 \times 10^{-4}$ emu mol^{-1}) and the χ_M plot in the SmC phase on the cooling run ($\theta \approx +30$ K, $C \approx 0.4$ emu K mol^{-1} between 83 and 67 °C if the Curie−Weiss law were applicable with the average χ_{dia}, -2.26×10^{-4} emu mol^{-1}, obtained by χ_M-T^{-1} plots in this narrow temperature range, although $T \gg \theta$ is the mandatory requirement to determine the χ_{dia} by χ_M-T^{-1} plots) (Figure S2a,b).[13] Although the average χ_{dia} used for the SmC phase is not accurate due to the temperature dependence and the too large θ value, such a small increase (0.50×10^{-4} emu mol^{-1}, 5%) in the χ_{dia} at the Cr-to-SmC transition is comparable to the magnitude of $\Delta\chi_{dia}$ observed in ordinary diamagnetic organic liquid crystals.[15] Thus, the overall χ_M increase (16%) observed at the Cr-to-SmC transition of (±)-**1a** was much larger than this χ_{dia} increase (5%) and includes a considerable net χ_{para} increase (11%).

However, since the scatter of the χ_M-T plots for **1a** and **1b** at higher temperatures was too large to discuss the details of the temperature dependence of the NPM (Figures S2−S5) and it was impossible to accurately estimate the χ_{para} values in the PLC materials due to the variable χ_{dia}, we have switched to measuring the χ_{para} values by EPR spectroscopy which allows us to ignore the χ_{dia} term.

EPR Spectroscopy. The temperature dependence of EPR spectra for **1a** and **1b** between 25 and 115 °C was measured at a magnetic field of 0.33 T (X-band) by using a quartz tube (5 mm ϕ). All of the EPR spectra obtained for **1a** and **1b** were Lorentzian in an ambient temperature range as previously reported (Figures S7−S10).[12,14,17] Therefore, by using the parameters directly obtained from the differential curves, such as maximum peak height (I'_m and $-I'_m$), g-value (g), and peak-to-peak line width (ΔH_{pp}), χ_{para} could be derived from the Bloch equation (eq 1).[18]

$$\chi_{para} = \frac{2\mu_B g I'_m \Delta H_{pp}^2}{\sqrt{3} h \nu H_1} \quad (1)$$

where μ_B is the Bohr magneton, h is Planck's constant, ν is the frequency of the absorbed electromagnetic wave, and H_1 is the amplitude of the oscillating magnetic field.

The temperature dependence of relative paramagnetic susceptibility (χ_{rel}), which is defined as

(16) (a) Mandel, S. K.; Nath, T. K.; Das, A.; Kremer, R. K. *Appl. Phys. Lett.* **2006**, *89*, 162502. (b) Schneider, J.; Handstein, A.; Zaveta, K. *J. Magn. Magn. Mater.* **1984**, *42*, 73–88.

(17) (a) Noda, Y.; Shimono, S.; Baba, M.; Yamauchi, J.; Ikuma, N.; Tamura, R. *J. Phys. Chem. B* **2006**, *110*, 23683–23687. (b) Noda, Y.; Shimono, S.; Baba, M.; Yamauchi, J.; Uchida, Y.; Ikuma, N.; Tamura, R. *Appl. Magn. Reson.* **2008**, *33*, 251–267.

(18) Bloch, F. *Phys. Rev.* **1946**, *70*, 460–474.

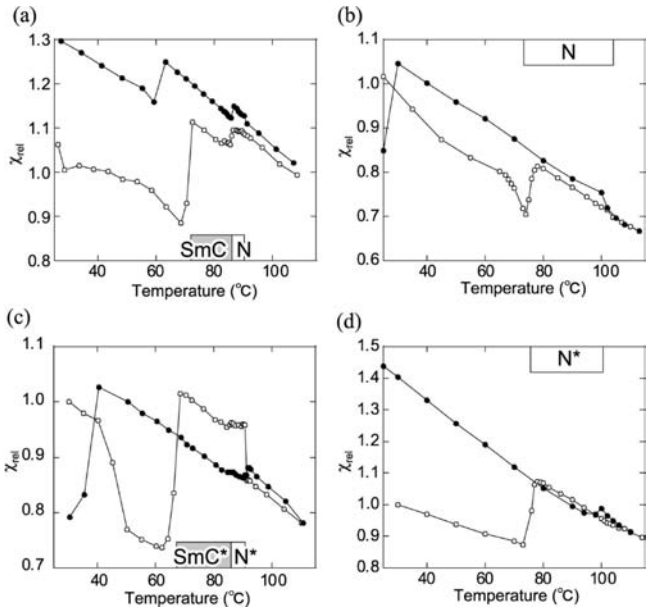

Figure 3. Temperature dependence of relative paramagnetic susceptibility (χ_{rel}) for (a) (±)-**1a**, (b) (±)-**1b**, (c) (2*S*,5*S*)-enriched **1a**, and (d) (2*S*,5*S*)-enriched **1b** at a magnetic field of 0.33 T. Open and filled circles represent the first heating and cooling runs, respectively. Error bars are not shown because they are sufficiently small. The LC temperatures shown in a box, which were determined by DSC analysis at a scanning rate of 5 °C min^{-1}, refer to the first heating process.

$$\chi_{rel} = \frac{\chi_{para}}{\chi_0} \tag{2}$$

where χ_0 is the standard paramagnetic susceptibility at 30 °C in the heating run, for (±)-**1a**, (±)-**1b**, (2*S*,5*S*)-enriched **1a**, and (2*S*,5*S*)-enriched **1b**, is shown in Figure 3. The magnetic data are the mean values of five measurements at each temperature to estimate χ_{para} with maximum accuracy. Although these magnetic data showed the same tendency as the results obtained by SQUID magnetization measurement (Figures S2−S5),[13] those obtained by EPR spectroscopy could show a more detailed change in χ_{para} with full reproducibility.

Racemic **1a** exhibited a χ_{rel} increase of 0.23 at the Cr-to-SmC phase transition (72 °C) and of 0.03 at the SmC-to-N transition (86 °C) in the heating run (Figure 3a). During the cooling process, the χ_{rel} of (±)-**1a** increased by 0.02 at the Iso-to-N transition (89 °C), decreased by 0.03 at the N-to-SmC transition (84 °C), and decreased by 0.09 at the SmC-to-Cr transition (62 °C) which occurred at a higher temperature in a quartz tube than in an Al pan used for differential scanning calorimetry (DSC) analysis (Figure 1). The χ_{rel} values in the SmC and N phases in the cooling run were larger than those in the heating run, indicating the large difference in the magnetic structure of the same PLC phases between the two processes.

In the case of (±)-**1b**, during the heating process, first the χ_{rel} decrease occurred at the Cr-to-Cr polymorphic transition temperature (67 °C) (Figures 3b, S3, and S6a). Then the χ_{rel} increased by 0.11 at the Cr-to-N transition (73 °C). During the cooling process, the χ_{rel} of (±)-**1b** increased by 0.03 at the Iso-to-N transition (102 °C) and finally decreased at the supercooled N-to-Cr transition (<30 °C). The χ_{rel} values in the N phase of (±)-**1b** on the cooling run were slightly larger than those in the heating run, indicating the small difference in the magnetic structure of the same paramagnetic N phase between the two processes.

(2*S*,5*S*)-Enriched **1a** showed a behavior different from (±)-**1a**. During the heating process, first the χ_{rel} decrease occurred at the Cr-to-Cr polymorphic transition temperature (49 °C) (Figures 3c and S6b). Then the χ_{rel} increased by 0.28 at the Cr-to-SmC* transition (67 °C), increased by 0.01 at the SmC*-to-N* phase transition (86 °C), and decreased by 0.10 at the N*-to-Iso transition (91 °C) (Figures 3c and S4). During the cooling process, the χ_{rel} decreased slightly by 0.01 and 0.001 at the Iso-to-N* and N*-to-SmC* transitions (90 and 85 °C), respectively; this former slight decrease is in contrast to the slight χ_{rel} increase (0.02) at the Iso-to-N transition of (±)-**1a**. The χ_{rel} values in the SmC* and N* phases on the cooling run were smaller than those in the heating run, indicating the large difference in the magnetic structure of the same PLC phases between the two processes.

In the case of (2*S*,5*S*)-enriched **1b**, during the heating process, the χ_{rel} increased by 0.20 at the Cr-to-N* transition (76 °C), similarly to the case of (±)-**1b** (Figures 3d and S5). During the cooling process, the χ_{rel} decreased by 0.02 at the Iso-to-N* phase transition (99 °C), similarly to the case of (2*S*,5*S*)-enriched **1a**. In contrast to other LC phases, the χ_{rel} values in the same paramagnetic N* phase in the heating and cooling runs were almost identical.

Thus, all of these four samples showed a considerable net χ_{rel} increase at the Cr-to-LC phase transition in the heating run similarly to the case of SQUID magnetometry (Figures S2−S5), while a very small change in the χ_{rel} value was commonly noted at the Iso-to-LC phase transition on the cooling run. This latter result implies the fair similarity in the magnetic local structure between the LC and Iso phases to hold an analogous magnetic interaction, which has never been reported in the field of molecular magnetism of a purely organic solid state at high temperatures.[19] Generally it is recognized that a rigid molecular ordering in a paramagnetic crystal leads to a uniform intermolecular magnetic interaction. However, in our work, a molecular fluctuation in both LC and Iso phases leading to nonuniform intermolecular contacts seems to afford an inhomogeneous intermolecular magnetic interaction. It is most likely that the interplay of such an inhomogeneous magnetic interaction and the low probability of intermolecular SOMO−SOMO overlapping, the latter of which is very often responsible for the generation of intermolecular antiferromagnetic interactions, would result in the generation of NPM in the LC phases of **1a** and **1b**.

Effects of LC Domain Size on Magnetic Interaction. Unexpectedly we observed the large difference and opposite tendency in the χ_{rel} value in the same LC phases of (±)-**1a** or (2*S*,5*S*)-enriched **1a** between the heating and cooling runs (Figure 3a,c), while only a slight difference in the χ_{rel} value was noted between the heating and cooling runs for the N or N* phase of **1b** (Figure 3b,d). Since such phenomena were quite unusual, we compared individual LC textures under random conditions between the heating and cooling runs by polarized optical microscopy. Consequently, we found that (i) in the SmC and N phases of (±)-**1a**, the Schlieren textures with larger and clearer multidomains were seen in the cooling run rather than in the heating one (Figure 4a,b); (ii) in the SmC* phase of (2*S*,5*S*)-enriched **1a**, the domain structure texture with a very large domain size was detected in the heating run, while the Schlieren texture with fine multidomains was seen on the cooling one (Figure 4c); (iii) in the N* phase of (2*S*,5*S*)-enriched **1a**, analogous fan-like

(19) *Magnetism: Molecules to Materials II*; Miller, J. S., Drillon, M., Eds.; Wiley-VCH: Weinheim, 2001.

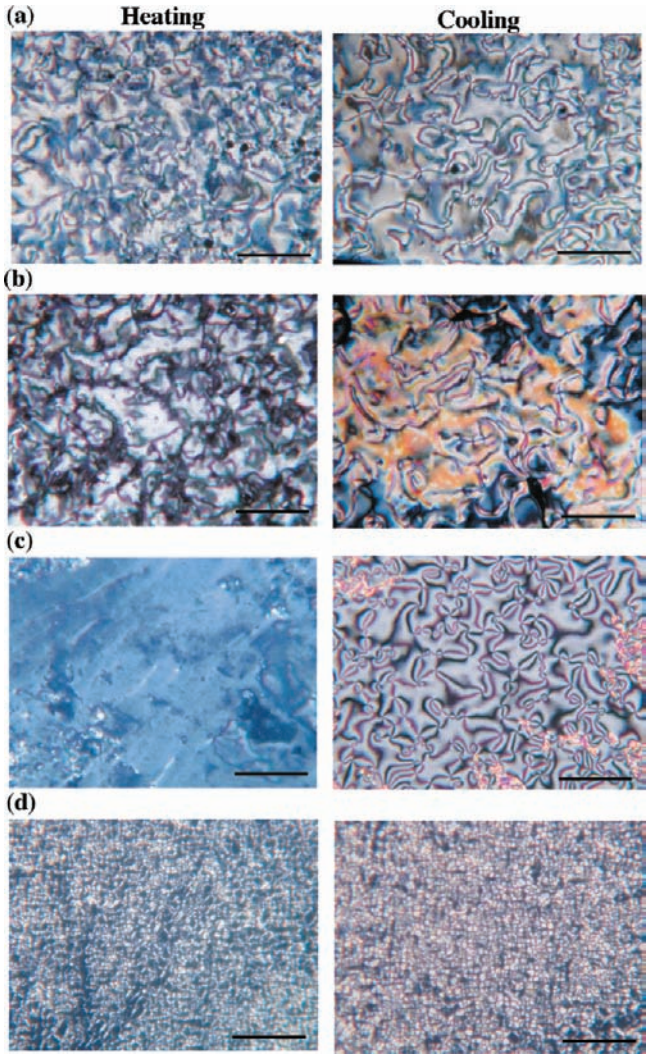

Figure 4. Comparison of individual LC textures of **1a** between the heating (left) and cooling (right) processes. (a) SmC phase at 82 °C; (b) N phase at 87 °C; (c) SmC* phase at 82 °C; (d) N* phase at 87 °C. Polarized optical photographs were taken under random conditions. The scale bar at the lower right in each photograph corresponds to 100 μm.

textures with a similar domain size were observed in the heating and cooling runs (Figure 4d); and (iv) in the N and N* phases of **1b**, no big difference in the domain size was noted between the heating and cooling runs. Accordingly, these results indicate that (i) the LC domain size is closely associated with the magnitude of overall magnetic interaction induced in the PLC phases—the larger each domain size is, the larger the overall magnetic interaction is—and that (ii) at the SmC-to-N or SmC*-to-N* phase transition the magnetic interaction induced in the N or N* phase is strongly affected by that in the preceding SmC or SmC* phase, respectively, and vice versa.

Origin of the NPM Observed in the PLC Phases. In this section, we first reveal that the molecular reorientation effect arising from the simple molecular magnetic anisotropy ($\Delta\chi$) has nothing to do with the NPM observed in the LC phases of **1a** and **1b**. Then we discuss the origin of the NPM in terms of the generation of a magnetic interaction involving the anisotropy of the spin−spin dipole interaction which originates from the LC superstructural anisotropy.

The contribution of $\Delta\chi$ can be expressed as the change in *g*-value owing to magnetic-field-induced molecular reorientation. It is well-known that χ_{para} is proportional to g^2 (eq 3).[9,14]

$$\chi_{para} = \frac{Ng^2\mu_B^2 S(S+1)}{3k(T-\theta)} \quad (3)$$

where N is Avogadro's constant, S is the spin quantum number, k is Boltzmann's constant, T is the temperature, and θ is Weiss' constant. Therefore, we examined the temperature dependence of the *g*-value for **1a** and **1b** by EPR spectroscopy at a magnetic field of 0.33 T (Figure 5a−d). If the change in *g*-value were primarily responsible for the NPM observed in the LC phases of **1a** and **1b**, (i) almost no χ_{rel} increase would be observed at the Cr-to-LC phase transition for (±)-**1a** because of the very small *g* increase (0.01%) (Figure 5a) and (ii) a χ_{rel} decrease should occur at the Cr-to-LC phase transition for (±)-**1b** and (2*S*,5*S*)-enriched **1a** and **1b** because of their *g* decrease (Figure 5b−d). Accordingly, it is concluded that the $\Delta\chi$ does not contribute to the NPM observed in the LC phases of **1a** and **1b** (Figure 2).

Next, we investigated the contribution of the LC superstructural anisotropy to the generation of intermolecular magnetic interaction. Generally, intermolecular magnetic interactions are divided into two factors, (a) spin−spin exchange interaction and (b) spin−spin dipole interaction. It is well-known that the magnetic ordering in organic radical crystals occurs at very low temperatures, where the spin−spin exchange interaction can overcome the thermal fluctuation[19] and a spin easy axis is produced as a result of the spin−spin dipole interaction.[20] Therefore, in analogy of this statement, it is easily expected that the spin−spin exchange and dipole interactions may operate in the LC phases of **1a** and **1b** even at high temperatures so as to produce a spin easy axis. To discuss the existence of the spin easy axis or the anisotropy of intermolecular magnetic interactions in the LC phases of **1a** and **1b**, the temperature dependence of ΔH_{pp} was compared with that of the *g*-value for **1a** and **1b** (Figure 5).

Fortunately, we could observe a slight but distinct difference in the ΔH_{pp} value in the SmC phase of a bulk sample of (±)-**1a** between the heating and cooling runs, although such a clear difference was not noted in the N, N*, and SmC* phases of **1a** and **1b** (Figure 5e−h). This difference in the ΔH_{pp} value in the SmC phase is considered to strongly correlate with that in the *g*-value, or the molecular orientation, between the heating and cooling runs in the magnetic field. Indeed, the distinct *g*-value change by 0.0004 between the two processes suggests the occurrence of molecular reorientation in the SmC phase qualitatively (Figure 5a); the SmC layer normal (*z*-axis in Figure 6a) somewhat showed the tendency to become perpendicular or parallel to the applied magnetic field in the heating or cooling run, respectively, because the molecular orientation was fairly influenced by the preceding Cr or N phase, as previously reported.[14] Thus, the difference in the ΔH_{pp} value in the same SmC phase between the heating and cooling runs should result from that in the molecular orientation in the LC phase. In other words, the difference in the ΔH_{pp} value is most likely attributed to the anisotropy of the spin−spin dipole interaction, because the spin−spin exchange interaction must be isotropic in the same LC phase at the same temperatures. Therefore, it is most likely that such an anisotropy of the spin−spin dipole interaction in the SmC phase leads to the formation of a spin easy axis, which must be parallel to the layer normal rather than the layer in the SmC phase for the reason described below.

To elucidate the origin and direction of the anisotropy of the spin−spin dipole interaction in the SmC phase, we briefly

(20) Kawamoto, T.; Suzuki, N. *J. Phys. Soc. Jpn.* **1994**, *63*, 3158–3162.

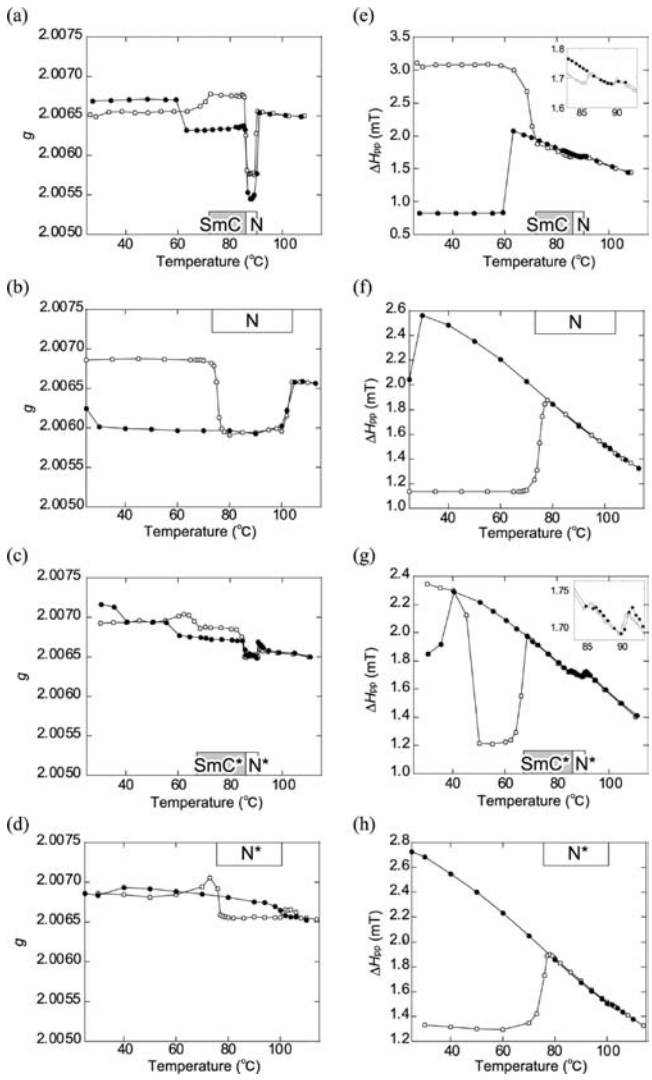

Figure 5. Temperature (T) dependences of g-value and ΔH_{pp} for **1a** and **1b** by EPR spectroscopy. At a field of 0.33 T in a temperature range of 25 to 115 °C. (a and e) (±)-**1a**; (b and f) (±)-**1b**; (c and g) (2*S*,5*S*)-enriched **1a**; (d and h) (2*S*,5*S*)-enriched **1b**. Open and filled circles represent the first heating and cooling runs, respectively. The insets in panels e and g indicate the magnification of the ΔH_{pp} *vs* T plots in the temperature range of 83 to 93 °C. The LC temperatures shown in a box, which were determined by DSC analysis at a scanning rate of 5 °C min^{-1}, refer to the first heating process.

discuss the correlation between the spin−spin dipole interaction and the SmC superstructure. On one hand, when the side-by-side spin−spin dipole interaction is operative, an antiferromagnetic interaction is more stable than a ferromagnetic one (Figure 6b,c). On the other hand, a ferromagnetic interaction is more stable than an antiferromagnetic one when the head-to-tail spin−spin dipole interaction operates (Figure 6d,e). Since a spin is localized on the nitroxyl group (N−O) in our PLC molecules (Figure 1) and a molecule would make contact with adjacent molecules anisotropically in the SmC layer (Figure 6f), the spin−spin dipole interaction parallel to the layer normal should be favored to result in the generation of a spin easy axis along the layer normal. Thus, the LC superstructural anisotropy can induce the anisotropy of the spin−spin dipole interaction, eventually leading to the generation of the anisotropic and inhomogeneous magnetic interaction, or the NPM, in the PLC phases.

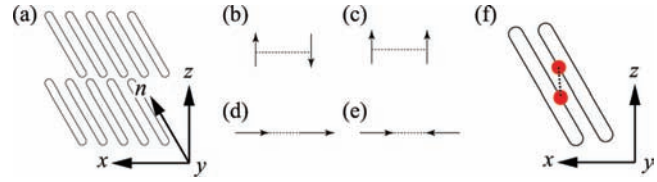

Figure 6. Schematic representation of the spin−spin dipole interaction in a paramagnetic SmC phase. (a) Rod-like molecules form layer ($x-y$ plane) structures in the SmC phase, and their director (n) is not parallel to the layer normal (z-axis). (b−e) Possible spin−spin dipole interactions between two spins. A magnetic field is applied perpendicular to the direction of the side-by-side interaction between two spins in (b) and (c), while it is applied parallel to the direction of the head-to-tail interaction between two spins in (d) and (e). (f) Spin−spin interaction between spins (red circles) localized in radical moieties in the SmC phase.

As far as the bulk samples of **1a** and **1b** were employed, an appreciable anisotropy of the spin−spin dipole interaction, which corresponds to the difference in the ΔH_{pp} value between the heating and cooling runs was observed only for the SmC phase of (±)-**1a**. Previously we reported that the majority of molecules align their long axis along the applied magnetic field of 0.33 T in the N phase of (±)-**1a**,[14] and we have confirmed that the peculiar helical superstructure is not unwound at all at 0.33 T in both SmC* and N* phases of (2*S*,5*S*)-enriched **1a**. These properties regarding molecular orientation would be responsible for no observation of the anisotropy of the spin−spin dipole interaction in the N, SmC*, and N* phases with multidomains of bulk samples (Figure 5b−d). Nevertheless, if these samples are introduced into a thin sandwich cell with the inner surface treatment so as to define the molecular alignment as homogeneous or homeotropic, the unique anisotropy in the ΔH_{pp} value as well as in the g and χ_{rel} values, depending on the type of LC superstructures, would be observed by VT-EPR spectroscopy.

Motion of LC Droplets on Water under the Influence of a Permanent Magnet. To compare the extents of the NPM in various LC phases visually, we examined how individual LC droplets and crystallized particles of racemic and (2*S*,5*S*)-enriched **1a** and **1b** on water behaved under the influence of a permanent magnet. The LC droplet with a diameter of 1−5 mm was prepared by floating the melted LC compound on hot water at 73 °C by using a small plastic spatula. Generally, a sufficiently strong magnet can attract any paramagnetic materials. As a rod-like rare-earth magnet (maximum 0.5 T, 6 mm $\phi \times$ 20 mm) approached (Figure 7a), all of the four LC droplets (SmC, SmC*, N, and N*) of racemic and (2*S*,5*S*)-enriched **1a** and **1b** floating on water were explicitly attracted by both the N and S poles of the magnet (Figure 7b and Movies S1−S4), whereas the four crystallized particles on water never moved under the influence of the same magnet. This behavior was fully reproducible. These results indicate that the threshold magnetic field required to attract crystalline particles with the magnet is larger than that required for attracting LC droplets. Here it should be stressed that the $\Delta\chi_{dia}$-controlled molecular reorientation originated from the Freedericksz effect in the PLC phases[14] cannot be responsible for the translation of LC droplets on water, which is controlled by the magnitude and sign of their χ values.

We should consider two factors to explain the difference in the response to the magnet between the LC droplets and crystallized particles of **1a** and **1b**; one is the magnitude of the interfacial interaction between the droplet or particle and water, and the other is that of NPM. First let us consider the effects of interfacial interaction. For reference, a diamagnetic LC droplet was prepared in a similar manner from the commercially

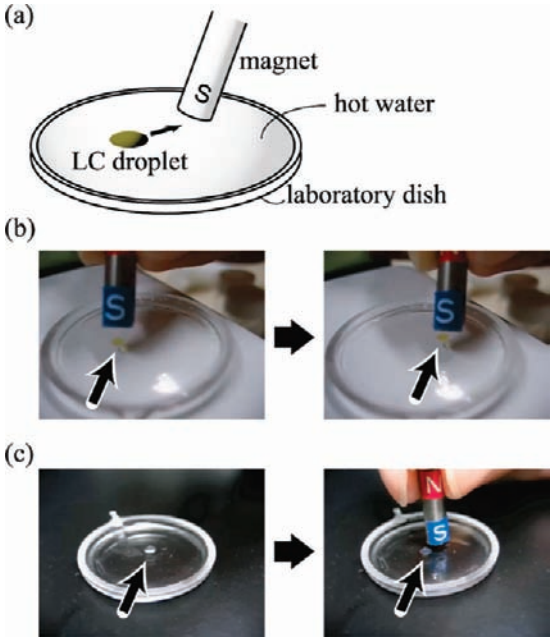

Figure 7. Motion of LC droplets on water under the action of a permanent magnet (maximum 0.5 T). (a) Schematic representation of the experimental setup for observing the attraction by a permanent magnet of a paramagnetic LC droplet on water in a shallow laboratory dish. (b) Photographs showing the attraction of the yellow paramagnetic N droplet of (±)-**1b** on water at 73 °C to the magnet. (c) Photographs showing the repulsion of the white diamagnetic N droplet of ZLI-1132 (Merck) on water at 25 °C from the magnet. Movies S1, S2, S3, S4, and S5 in an MPEG format in the Supporting Information show the motion of LC droplets of (±)-**1a**, (±)-**1b**, (2*S*,5*S*)-enriched **1a**, (2*S*,5*S*)-enriched **1b**, and ZLI-1132, respectively.

available compounds mixture (Merck ZLI-1132), which shows an N phase below 70 °C (<25 N 71.9 Iso). In contrast to **1a** and **1b**, the diamagnetic LC droplet on water at 25 °C or higher temperatures was slowly repelled by the same magnet (Figure 7c and Movie S5). This repulsion is most likely due to the negative χ of ZLI-1132, whereas the former attraction of **1a** and **1b** should arise from the positive χ. Therefore, the smaller interfacial interaction between the LC droplet and water compared to that between the crystallized particle and water seems to allow the LC droplet to move on water under the influence of the magnet, irrespective of either attractive or repulsive motion.

More interestingly, the N*, SmC, and SmC* droplets quickly responded to the influence of the magnet, while the N droplet moved slowly (Movies S1−S4). Furthermore, unexpectedly we observed that for all four different droplets the larger the droplet size is, the faster the response is. These results suggest that the difference in the response of these LC droplets to the magnet should depend not only on the interfacial interaction between the LC droplet and water but also on the magnitude of NPM.

As expected, the difference in the χ_{rel} value for the four LC phases of **1a** and **1b** at 73 °C on the cooling run was consistent with that in the response of four LC droplets to the action of a permanent magnet (Figure 7). The χ_{rel} value in the N phase and the χ_{rel} increase at the Cr-to-N phase transition with respect to (±)-**1b** were smaller than those in the SmC phase of (±)-**1a**, the SmC* phase of (2*S*,5*S*)-enriched **1a**, or the N* phase of (2*S*,5*S*)-enriched **1b** (Figure 3). These results suggest that the slowest response of the N droplet of (±)-**1b** to the magnet corresponds to the smallest χ_{rel} value, i.e., the smallest NPM.

Conclusions

By SQUID magnetometry and VT-EPR spectroscopy, the NPM in various PLC phases of **1a** and **1b** was discovered to arise from the anisotropic and inhomogeneous magnetic interaction ($\bar{J} > 0$) that originates from the formation of magnetic local structures or domains induced by LC superstructures. In this process, we showed that EPR spectroscopy is an appropriate means for the measurement of temperature dependence of χ_{para} for organic nitroxide monoradical LC phases at high temperatures between 25 and 115 °C, because (i) the treatment of the χ_{dia} term is unnecessary, (ii) the experimental error is very small even at high temperatures, and (iii) the information on microscopic magnetic interactions such as spin−spin dipole and exchange interactions is available, too.

In-depth understanding of such an anisotropic and inhomogeneous magnetic interaction ($\bar{J} > 0$) may lead to the development of totally new all-organic magnetic LC materials. For example, the use as a metal-free magnetic carrier for a magnetically targeted drug-delivery system in place of magnetoliposomes containing Fe_3O_4 is promising, because it is known that stable free radical nitroxides are nontoxic to cells and animals and can serve as potent antioxidants possessing superoxide dismutase- and catalase-mimetic activity that can protect cells and animals against a variety of oxidative effects.[21] Alternatively, since the SmC* phase of **1a** exhibited some magnetic ordering in a weak magnetic field, it is highly expected to detect the magneto-electric effects in the FLC state of **1a** and analogous compounds.[7,12,22]

Experimental Section

Sample Preparation of LC Droplets and Observation of Their Response to a Magnet. To make the LC droplets (1−5 mm ϕ) of **1**, each powder sample (2−3 mg) was melted at 100 °C and the resulting viscous liquid was floated on hot water (73 °C) by a small plastic spatula. For ZLI-1132, the LC sample was floated on water by a pipet at room temperature. A thin laboratory dish (34 mm ϕ × 2 mm) was used for the container of the droplets. The observation of LC droplets on water was performed at 73 °C for **1** or 25 °C for ZLI-1132. A rod-like rare-earth magnet (maximum 0.5 T, 6 mm ϕ × 20 mm, Kenis KD-1) was utilized for observervation of droplet response on water.

Acknowledgment. We thank Professors W. Haase and T. Takui for helpful advice. This work was supported by the Grant-in-Aid for Scientific Research (No. 19350067) from Japan Society for the Promotion of Science (JSPS), the Asahi Glass Foundation (to R.T.), and the Murata Science Foundation (to Y.U.). Y.U. is very grateful to the JSPS Research Fellowships for Young Scientists.

Supporting Information Available: Figures S1−S10 and Movies S1−S5. This material is available free of charge via the Internet at http://pubs.acs.org.

JA101930D

(21) (a) Mitchell, J. B.; Xavier, S.; DeLuca, A. M.; Sowers, A. L.; Cook, J. A.; Krishna, M. C.; Hahn, S. M.; Russo, A. *Free Radical Biol. Med.* **2003**, *34*, 93–102. (b) Arieli, D.; Nahmany, G.; Casap, N.; Ad-El, D.; Samuni, Y. *Free Radical Res.* **2008**, *42*, 114–123.

(22) (a) Uchida, Y.; Tamura, R.; Ikuma, N.; Shimono, S.; Yamauchi, J.; Aoki, Y.; Nohira, H. *Mol. Cryst. Liq. Cryst.* **2007**, *479*, 213–221. (b) Uchida, Y.; Tamura, R.; Ikuma, N.; Yamauchi, J.; Aoki, Y.; Nohira, H. *Ferroelectrics* **2008**, *365*, 158–169.